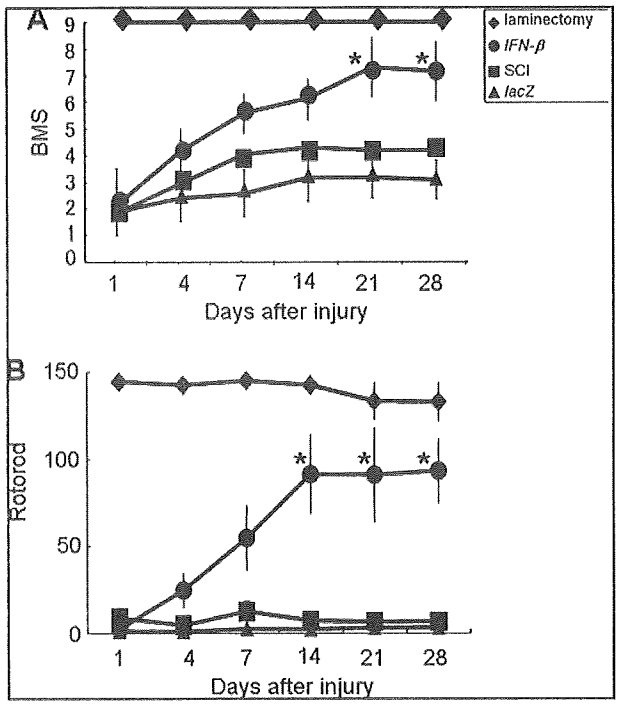

FIG. 6. Behavioral studies. We assessed functional recovery by employing two independent behavioral tasks: the BMS score (A) and the rotarod test (B). All injured animals, except those in the laminectomy group, exhibited a mean BMS score of 2 on the first day post-SCI. Animals with plain SCI receiving no control agents (plain SCI group) and those receiving the *lacZ* control vector (*lacZ*-treated group) spontaneously recovered to a BMS score of 3–4 until 14 days post-injury, and no further recovery was observed thereafter. On the other hand, the IFN-β-treated animals showed a significant improvement in the BMS, relative to the control groups. On an average, the IFN-β-treated group exhibited a mean BMS score of 7.1 ± 1.1 at 28 days, while the plain SCI and the *lacZ*-treated groups attained a mean score of 4.2 ± 0.3 and 3.1 ± 0.7, respectively. Rotarod analysis was performed to examine another locomotor function after SCI. The animals were evaluated for locomotor recovery on days 1, 4, 7, 14, 21, and 28. There was significant recovery in performance over 14 days post-injury in the IFN-β-treated group, while the performance was severely impaired in the plain SCI and *lacZ*-treated animals at all time points. $^*p < 0.05$, compared to the plain SCI and *lacZ* groups. The data are expressed as means $\pm$ SD of eight animals tested.

degeneration following SCI (Faulkner et al., 2004). This evidence indicates that the glial scar might provide certain beneficial effects to stabilize CNS tissue after injury. However, this benefit of glial scarring may only be observed in the acute phase after injury. In the subacute phase, many astrocytes in the injured area become hyperplastic and adopt a reactive phenotype to release an inhibitory extracellular matrix comprising components such as chondroitin sulfate proteoglycans (CSPGs) (Silver and Miller, 2004). The biochemical hallmark of reactive astrocytes is the massive upregulation of the GFAP intermediate filament protein (Barrett et al., 1981; Eng, 1985). The reactive astrocytes form a dense network of glial processes extending from the lesion site.

At the start of this study, the time course of glial scar formation following SCI was evaluated by immunohistochemistry with anti-GFAP antibody (Supplementary Fig. 1A online only). The total number of GFAP-expressing astrocytes was counted in a 0.25-mm^2 grid at the lesion site in every third serial longitudinal 8-μm section (Supplementary Fig. 1B online only). This injury gradually led to hyperplasticity of the GFAP-positive cells. On day 14, the vast majority of GFAP-positive astrocytes at the lesion site was hyperplastic and stained very strongly with GFAP. GFAP-positive scar-forming astrocytes were spreading at a certain distance from the original wound. At the site of dorsal column hemisection, cavitation was also observed. These findings were consistent with those of a previous report (Okada et al., 2006). Therefore, molecular signaling mechanisms involved in the development of reactive astrocytes can be obtained at the subacute phase of SCI, before the glial scar is established. Although a number of SCI-related studies have employed comprehensive microarray analyses to examine the gene expression changes induced by SCI (Aimone et al., 2004; Schmitt et al., 2006; Song et al., 2001; Yang et al., 2006), the specificity of the reactive astrocytes responding to SCI has not been well addressed. Thus we attempted to identify profile changes in the gene expression in astrocytic gliosis at 10 days post-injury by using fine laser-captured microdissection, genome-wide microarray, and MetaCore pathway analysis. This systematic processing revealed many intriguing activated pathways that were statistically significant ($p < 0.05$), including those involved in ECM remodeling, cytoskeleton remodeling, and the myelin-associated glycoprotein (MAG)-dependent inhibition of neurite outgrowths (Fig. 1). These pathways will be discussed in greater detail in a separate article. In brief, our finding is consistent with evidence provided by studies that prove that the expression of ECM molecules termed CSPGs (aggrecan, brevican, neurocan, versican, phosphacan, and NG2) is rapidly upregulated by reactive astrocytes after injury, forming an inhibitory gradient across the axons (McKeon et al., 1991), that the hypertrophic reactive astrocytes responding to injury produce large amounts of intermediate filaments such as GFAP and vimentin (Barrett et al., 1981; Bignami and Dahl, 1974; Eng, 1985; Yang et al., 1994), and that MAG release inhibits axon outgrowth (McKerracher et al., 1994; Mukhopadhyay et al., 1994). Provided that proliferation or mitosis is one of the most prominent features of reactive astrocytes, this study focused on another functional role of Ras family kinase cascades in reactive astrocytes, and on the therapeutic strategies for inhibiting the MEK/ERK-dependent proliferation of reactive gliosis following SCI. The Ras/Raf/MEK/ERK pathway is involved in the regulation of many fundamental cellular processes, including cell proliferation, survival, and differentiation (Chong et al., 2003; Kolch, 2005) (Fig. 1C). Primarily, many receptors induce Ras activation. Ras is a small GTPase that binds to and recruits Raf kinases to the cell membrane for subsequent activation. Activated Raf kinases are the entry points into a three-tiered kinase cascade in which Raf phosphorylates and activates MEK, which in turn phosphorylates and activates ERK. Raf has 3 isoforms (A-Raf, B-Raf, and Raf-1) that have distinct and specific functions. MEK—a downstream effector of the Ras/Raf/MEK/ERK pathway—is the only commonly accepted substrate of all the three isoforms of Raf, and ERK is the only known substrate of MEK. Both MEK and ERK have

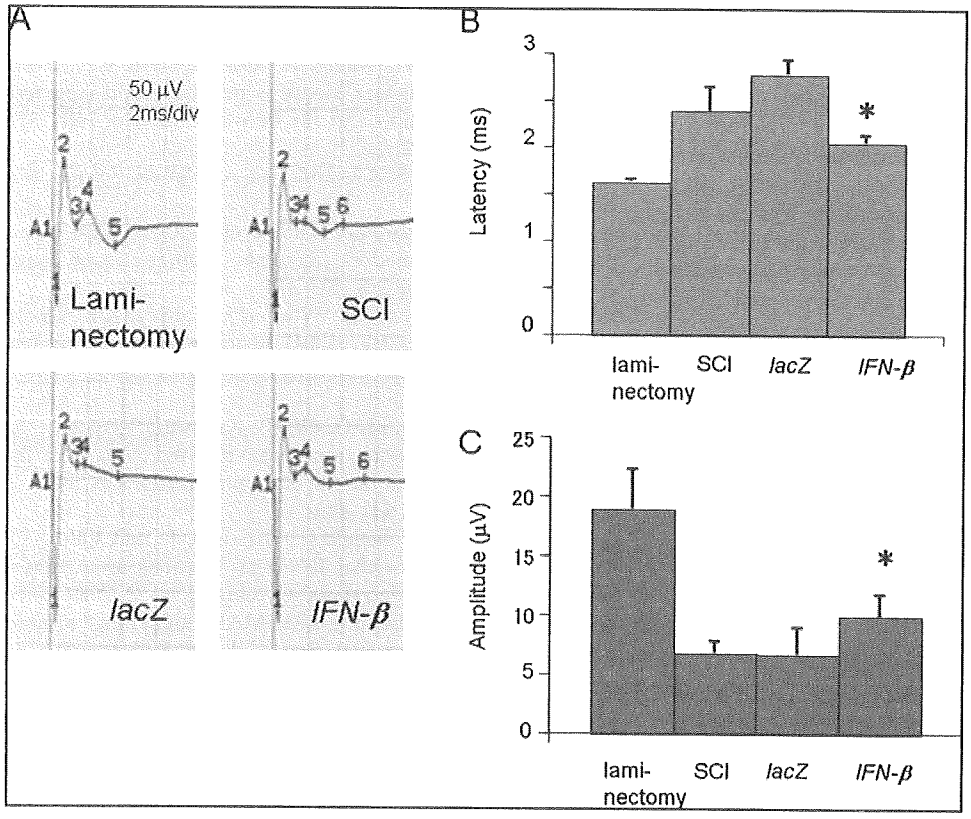

FIG. 7. Electrophysiology. Transcranial electrical motor nerve evoked-action potentials (MEPs) were measured from 28 days after injury. Electrical stimulation (1 Hz, 6 mA) was delivered over the cranium, 1 mm lateral to the bregma. The evoked responses were recorded from the contralateral femoral muscle. (**A**) Representative electrograms. The points numbered 1–5 were automatically drawn in each electrogram, and the numbers 1 and 2 were recognized as artifacts. Latency (**B**) was defined as the time elapsed between the onset of the stimulus and the initial deflection of the response from baseline (point 3). The amplitude (**C**) was measured from base to peak (from points 3 to 4). The data are expressed as means ± SD of five animals tested.

two isoforms in mammals (MEK1/2 and ERK1/2), which are co-regulated in most cases. Subsequently, ERK has >70 established substrates that include nuclear transcription factors, cytoskeletal and signaling proteins, and receptors (Roux and Blenis, 2004). Because MEK and ERK are considered to be the main effectors of this pathway, we validated the activation of Ras family signaling cascades by both functional phosphorylation and quantitative increase in MEK1/2 and ERK1/2 expression. Consequently, we confirmed that the MEK/ERK pathway is upregulated in reactive astrocytes after injury.

It is important to consider how MEK-ERK-dependent proliferation of reactive gliosis after injury can be inhibited. Considering the above-described double-edged roles of reactive astrocytes after SCI, an ideal strategy for SCI treatment might involve the inhibition of the aberrant development of hypertrophic reactive astrocytes without eliminating normal quiescent astrocytes that may serve to prevent a cascading wave of uncontrolled tissue damage. A potential strategy could be the use of IFNs. IFN-γ, one of the type II IFNs, reduced astrocyte CSPG production by 60%, suggesting that IFN can enhance axonal regeneration (Smith and Strunz, 2005). Type I IFNs (the IFN-α family and IFN-β) are known to inhibit tumor growth (Borden et al., 2000). In particular, IFN-β deserves attention as a cell-cycle regulator re-entering from aberrant cell-cycle progression to a senescence-like state (Kaynor et al., 2002). We have previously reported significant anti-tumor activity and improved survival in mouse glial neoplasm models by employing a liposome complex with a plasmid vector encoding IFN-β (Mizuno et al., 1990; Natsume et al., 1999; Natsume et al., 2000); further, a phase I/IIa clinical trial of IFN-β gene therapy for patients with malignant glial tumors has also been conducted (Yoshida et al., 2004).

Major research studies to help us understand the signaling mechanisms through which IFNs induce their effects have been undertaken. The regulatory signals triggered by type I IFNs are transduced to the nucleus via the JAK/STAT pathway, whereby ligand-activated JAK kinases phosphorylate STAT proteins, which subsequently dimerize and migrate to the nucleus to regulate gene expression (Darnell, 1997). In addition to the classical JAK/STAT pathway, there is evidence that other multiple distinct signaling cascades are required for generating the IFN responses (Platanias, 2005). Recently, it has been proven that IFNs block the constitutive activation of the MEK/ERK signaling pathway (Li et al., 2004; Romerio et al., 2000; Romerio and Zella, 2002; Zella et al., 2000). In this context, we hypothesized that IFN-β may block the proliferation of reactive astrocytes following SCI, and eventually promote axonal growth and functional recovery. Indeed, as shown in Fig. 2, liposome-mediated IFN-β gene delivery exerted an anti-proliferative effect on primary cultured astrocytes without ablating pre-existing ones. On the other hand, IFN-β gene delivery did not exert a neurotrophic effect on the neurons and PC12 cells in culture (data not shown). IFN-β protein demonstrated an extremely limited anti-proliferative effect on astrocytes. This finding is similar to that of our previous study, in which even repeated local injections of IFN-β protein (1000 IU) failed to suppress glial tumors in a mouse orthotopic model, although the IFN-β gene/liposome complex eradicated the tumor entirely. This may be due to the short half-life of IFNs (<60 min) that renders the achievement of sustained therapeutic levels difficult (Wilderman et al., 2005). As a delivery system, we took advantage of the unique characteristics of liposomes that have a high potential for DNA transfer into dividing cells (Yoshida and Mizuno, 2003).

In the SCI model used in this study, gene delivery appeared to possess certain specificity to target reactive gliosis. In animal experiments, liposome-mediated IFN-β gene delivery reduced glial scarring and promoted CST axonal regrowth when measured by labeling with the anterograde tracer biotinylated dextran amine (BDA). More importantly, this strategy remarkably improved the functional behavior and parameters of electrophysiology. We speculate that the deactivation of the MEK/ERK pathway is the mechanism of action associated with these findings, since we observed a decrease in the phosphorylation of the concerned molecules after IFN-β gene delivery. Further studies are warranted to elucidate the direct mechanism though which the deactivation of the MEK/ERK pathway inhibits the proliferation of reactive astrocytes. However, the results demonstrate that IFN-β gene delivery using liposomes is effective in blocking glial scarring, and thus our results support the possible use of IFN-β gene therapy for SCI.

Acknowledgements

This work was supported by a Grant-in-Aid for Scientific Research from the Ministry of Health, Labor, and Welfare. We are indebted to Dr. Atsumi Nitta of the Department of Neuropsychopharmacology, Nagoya University School of Medicine, for helpful suggestions about behavioral studies; Dr. Masaaki Hirayama of the Department of Neurology, Nagoya University School of Medicine, for supervising the electrophysiological studies; and to the Division of Clinical Pathology, Kariya Toyota General Hospital, for histological examination. We would like to thank Drs. Harley Kornblum at the University of California at Los Angeles, and David Fink at the University of Michigan in Ann Arbor for their constructive discussion.

Author Disclosure Statement

No conflicting financial interests exist.

References

Aimone, J.B., Leasure, J.L., Perreau, V.M., and Thallmair, M. (2004). Spatial and temporal gene expression profiling of the contused rat spinal cord. Exp. Neurol. 189, 204–221.

Barrett, C.P., Guth, L., Donati, E.J., and Krikorian, J.G. (1981). Astroglial reaction in the gray matter lumbar segments after midthoracic transection of the adult rat spinal cord. Exp. Neurol. 73, 365–377.

Basso, D.M., Fisher, L.C., Anderson, A.J., Jakeman, L.B., McTigue, D.M., and Popovich, P. G. (2006). Basso Mouse Scale for locomotion detects differences in recovery after spinal cord injury in five common mouse strains. J. Neurotrauma. 23, 635–659.

Bignami, A., and Dahl, D. (1974). Astrocyte-specific protein and neuroglial differentiation. An immunofluorescence study with antibodies to the glial fibrillary acidic protein. J. Comp. Neurol. 153, 27–38.

Borden, E.C., Lindner, D., Dreicer, R., Hussein, M., and Peereboom, D. (2000). Second-generation interferons for cancer: clinical targets. Semin. Cancer Biol. 10, 125–144.

Brunet, A., Pages, G., and Pouyssegur, J. (1994). Constitutively active mutants of MAP kinase kinase (MEK1) induce growth factor-relaxation and oncogenicity when expressed in fibroblasts. Oncogene 9, 3379–3387.

Chong, H., Vikis, H.G., and Guan, K.L. (2003). Mechanisms of regulating the Raf kinase family. Cell Signal 15, 463–469.

Cowley, S., Paterson, H., Kemp, P., and Marshall, C.J. (1994). Activation of MAP kinase kinase is necessary and sufficient for PC12 differentiation and for transformation of NIH 3T3 cells. Cell 77, 841–852.

Darnell, J.E., Jr. (1997). STATs and gene regulation. Science 277, 1630–1635.

Eng, L.F. (1985). Glial fibrillary acidic protein (GFAP): the major protein of glial intermediate filaments in differentiated astrocytes. J. Neuroimmunol. 8, 203–214.

Faulkner, J.R., Herrmann, J.E., Woo, M.J., Tansey, K.E., Doan, N.B., and Sofroniew, M.V. (2004). Reactive astrocytes protect tissue and preserve function after spinal cord injury. J. Neurosci. 24, 2143–2155.

Inman, D.M., and Steward, O. (2003). Ascending sensory, but not other long-tract axons, regenerate into the connective tissue matrix that forms at the site of a spinal cord injury in mice. J. Comp. Neurol. 462, 431–449.

Kaynor, C., Xin, M., Wakefield, J., Barsoum, J., and Qin, X.Q. (2002). Direct evidence that IFN-beta functions as a tumor-suppressor protein. J. Interferon Cytokine Res. 22, 1089–1098.

Kolch, W. (2005). Coordinating ERK/MAPK signalling through scaffolds and inhibitors. Nat. Rev. Mol. Cell Biol. 6, 827–837.

Li, C., Chi, S., He, N., Zhang, X., Guicherit, O., Wagner, R., Tyring, S., and Xie, J. (2004). IFNalpha induces Fas expression and apoptosis in hedgehog pathway activated BCC cells through inhibiting Ras-Erk signaling. Oncogene 23, 1608–1617.

Mansour, S.J., Matten, W.T., Hermann, A.S., Candia, J.M., Rong, S., Fukasawa, K., Vande Woude, G.F., and Ahn, N.G. (1994). Transformation of mammalian cells by constitutively active MAP kinase kinase. Science 265, 966–970.

McKeon, R.J., Schreiber, R.C., Rudge, J.S., and Silver, J. (1991). Reduction of neurite outgrowth in a model of glial scarring following CNS injury is correlated with the expression of inhibitory molecules on reactive astrocytes. J. Neurosci. 11, 3398–3411.

McKerracher, L., David, S., Jackson, D.L., Kottis, V., Dunn, R.J., and Braun, P.E. (1994). Identification of myelin-associated glycoprotein as a major myelin-derived inhibitor of neurite growth. Neuron 13, 805–811.

Mizuno, M., Yoshida, J., Sugita, K., Inoue, I., Seo, H., Hayashi, Y., Koshizaka, T., and Yagi, K. (1990). Growth inhibition of glioma cells transfected with the human beta-interferon gene by liposomes coupled with a monoclonal antibody. Cancer Res 50, 7826–7829.

Mukhopadhyay, G., Doherty, P., Walsh, F.S., Crocker, P.R., and Filbin, M.T. (1994). A novel role for myelin-associated glycoprotein as an inhibitor of axonal regeneration. Neuron 13, 757–767.

Natsume, A., Mizuno, M., Ryuke, Y., and Yoshida, J. (1999). Antitumor effect and cellular immunity activation by murine interferon-beta gene transfer against intracerebral glioma in mouse. Gene Ther. 6, 1626–1633.

Natsume, A., Tsujimura, K., Mizuno, M., Takahashi, T., and Yoshida, J. (2000). IFN-beta gene therapy induces systemic antitumor immunity against malignant glioma. J. Neurooncol. 47, 117–124.

Okada, S., Nakamura, M., Katoh, H., Miyao, T., Shimazaki, T., Ishii, K., Yamane, J., Yoshimura, A., Iwamoto, Y., Toyama, Y., and Okano, H. (2006). Conditional ablation of Stat3 or Socs3 discloses a dual role for reactive astrocytes after spinal cord injury. Nat. Med. 12, 829–834.

Okazaki, K., and Sagata, N. (1995). MAP kinase activation is essential for oncogenic transformation of NIH3T3 cells by Mos. Oncogene 10, 1149–1157.

Pages, G., Lenormand, P., L'Allemain, G., Chambard, J.C., Meloche, S., and Pouyssegur, J. (1993). Mitogen-activated protein kinases p42mapk and p44mapk are required for fibroblast proliferation. Proc. Natl. Acad. Sci. USA 90, 8319–8323.

Platanias, L.C. (2005). Mechanisms of type-I- and type-II-interferon-mediated signalling. Nat Rev Immunol 5, 375–386.

Pumiglia, K.M., and Decker, S.J. (1997). Cell cycle arrest mediated by the MEK/mitogen-activated protein kinase pathway. Proc. Natl. Acad. Sci. USA 94, 448–452.

Romerio, F., and Zella, D. (2002). MEK and ERK inhibitors enhance the anti-proliferative effect of interferon-alpha2b. FASEB J 16, 1680–1682.

Romerio, F., Riva, A., and Zella, D. (2000). Interferon-alpha2b reduces phosphorylation and activity of MEK and ERK through a Ras/Raf-independent mechanism. Br. J. Cancer 83, 532–538.

Roux, P.P., and Blenis, J. (2004). ERK and p38 MAPK-activated protein kinases: a family of protein kinases with diverse biological functions. Microbiol. Mol. Biol. Rev. 68, 320–344.

Schmitt, C., Miranpuri, G.S., Dhodda, V.K., Isaacson, J., Vemuganti, R., and Resnick, D.K. (2006). Changes in spinal cord injury-induced gene expression in rat are strain-dependent. Spine J. 6, 113–119.

Seger, R., and Krebs, E.G. (1995). The MAPK signaling cascade. FASEB J 9, 726–735.

Seger, R., Seger, D., Reszka, A.A., Munar, E.S., Eldar-Finkelman, H., Dobrowolska, G., Jensen, A.M., Campbell, J.S., Fischer, E.H., and Krebs, E.G. (1994). Overexpression of mitogen-activated protein kinase kinase (MAPKK) and its mutants in NIH 3T3 cells. Evidence that MAPKK involvement in cellular proliferation is regulated by phosphorylation of serine residues in its kinase subdomains VII and VIII. J. Biol. Chem. 269, 25699–25709.

Silver, J., and Miller, J.H. (2004). Regeneration beyond the glial scar. Nat. Rev. Neurosci. 5, 146–156.

Smith, G.M., and Strunz, C. (2005). Growth factor and cytokine regulation of chondroitin sulfate proteoglycans by astrocytes. Glia 52, 209–218.

Song, G., Cechvala, C., Resnick, D.K., Dempsey, R.J., and Rao, V.L. (2001). GeneChip analysis after acute spinal cord injury in rat. J. Neurochem. 79, 804–815.

Stark, G.R., Kerr, I.M., Williams, B.R., Silverman, R.H., and Schreiber, R.D. (1998). How cells respond to interferons. Annu. Rev. Biochem. 67, 227–264.

Stichel, C.C., and Muller, H.W. (1998). The CNS lesion scar: new vistas on an old regeneration barrier. Cell Tissue Res. 294, 1–9.

Traverse, S., Gomez, N., Paterson, H., Marshall, C., and Cohen, P. (1992). Sustained activation of the mitogen-activated protein (MAP) kinase cascade may be required for differentiation of PC12 cells. Comparison of the effects of nerve growth factor and epidermal growth factor. Biochem. J. 288(Pt 2), 351–355.

Webb, C.P., Van Aelst, L., Wigler, M.H., and Woude, G.F. (1998). Signaling pathways in Ras-mediated tumorigenicity and metastasis. Proc. Natl. Acad. Sci. USA 95, 8773–8778.

Wilderman, M.J., Sun, J., Jassar, A.S., Kapoor, V., Khan, M., Vachani, A., Suzuki, E., Kinniry, P.A., Sterman, D.H., Kaiser, L.R., and Albelda, S.M. (2005). Intrapulmonary IFN-beta gene therapy using an adenoviral vector is highly effective in a murine orthotopic model of bronchogenic adenocarcinoma of the lung. Cancer Res. 65, 8379–8387.

Yang, H.Y., Lieska, N., Shao, D., Kriho, V., and Pappas, G.D. (1994). Proteins of the intermediate filament cytoskeleton as markers for astrocytes and human astrocytomas. Mol. Chem. Neuropathol. 21, 155–176.

Yang, Y., Xie, Y., Chai, H., Fan, M., Liu, S., Liu, H., Bruce, I., and Wu, W. (2006). Microarray analysis of gene expression patterns in adult spinal motoneurons after different types of axonal injuries. Brain Res. 1075, 1–12.

Yoshida, J., and Mizuno, M. (2003). Clinical gene therapy for brain tumors. Liposomal delivery of anticancer molecule to glioma. J. Neurooncol. 65, 261–267.

Yoshida, J., Mizuno, M., Fujii, M., Kajita, Y., Nakahara, N., Hatano, M., Saito, R., Nobayashi, M., and Wakabayashi, T. (2004). Human gene therapy for malignant gliomas (glioblastoma multiforme and anaplastic astrocytoma) by *in vivo* transduction with human interferon beta gene using cationic liposomes. Hum. Gene Ther. 15, 77–86.

Zella, D., Romerio, F., Curreli, S., Secchiero, P., Cicala, C., Zagury, D., and Gallo, R.C. (2000). IFN-alpha 2b reduces IL-2 production and IL-2 receptor function in primary CD4+T cells. J. Immunol. 164, 2296–2302.

Address reprint requests to:
Atsushi Natsume, M.D.
Department of Neurosurgery
Nagoya University School of Medicine
65 Tsurumai-cho
Showa, Nagoya 466-8550, Aichi, Japan

E-mail: anatsume@med.nagoya-u.ac.jp

J Neurooncol
DOI 10.1007/s11060-008-9732-0

Synergistic induction of NY-ESO-1 antigen expression by a novel histone deacetylase inhibitor, valproic acid, with 5-aza-2′-deoxycytidine in glioma cells

Sachie Oi · Atsushi Natsume · Motokazu Ito · Yutaka Kondo · Shinji Shimato · Yuka Maeda · Kiyoshi Saito · Toshihiko Wakabayashi

Received: 25 June 2008 / Accepted: 3 November 2008

Abstract NY-ESO-1, one of the most immunogenic cancer/testis antigens, provides attractive targets for cancer immunotherapy. NY-ESO-1 has been demonstrated to be expressed in a range of solid tumors via DNA demethylation and/or histone modification; however, it has been rarely expressed in glioma. The reversibility of these epigenetic aberrations is potentially attractive for glioma treatment with DNA-methyltransferase inhibitors (DNMTi) and histone deacetylase inhibitors (HDACi), leading to reactivation of silenced genes. We previously demonstrated de novo induction of NY-ESO-1 in glioma cells by DNMTi. In this study, we show that an anticonvulsant, i.e., valproic acid (VPA), also acting as an HDACi, enhances induction of NY-ESO-1 in synergy with DNMTi. Chromatin assays demonstrated that combination of DNMTi and VPA elicited significant DNA demethylation, histone H3 Lys9 demethylation, and acetylation. These findings not only shed light on an epigenetic immunotherapy, but also suggest that the silencing of *NY-ESO-1* is mediated by histone modification.

Keywords NY-ESO-1 · DNA methylation · Histone deacetylase inhibitor · Glioma

S. Oi · A. Natsume (✉) · M. Ito · S. Shimato · Y. Maeda · K. Saito · T. Wakabayashi
Department of Neurosurgery, Nagoya University School of Medicine, Showa-ku, Nagoya 466-8550, Japan
e-mail: anatsume@med.nagoya-u.ac.jp

Y. Kondo
Division of Molecular Oncology, Aichi Cancer Center Research Institute, Chikusa-ku, Nagoya 464-8681, Japan

Published online: 22 November 2008

Introduction

Gliomas are the most common primary tumors of the central nervous system. They account for 30% of adult primary brain tumors. Brain tumors remain difficult to cure despite recent advances in surgical, radiotherapeutic, and chemotherapeutic managements. In particular, there is currently no optimal treatment for glioblastoma multiforme, which is the most common malignant brain tumor in adults, and patients typically survive for less than 1 year. This poor outcome partially relates to the inability to deliver chemotherapeutic agents across the blood–brain barrier (BBB) and the low effect of radiation on the tumor. Therefore, there is an urgent requirement for new and more effective strategies. Of these, the establishment of immunotherapy specifically targeting malignant cells is expected to improve tumor prognosis. A subgroup of tumor-specific antigens, frequently referred to as cancer/testis antigens (CTAs), are expressed only in the tissues of the testis, ovary, and placenta under normal conditions; however, they are also expressed in various types of human tumors [1, 2]. Since normal CTA-expressing tissues do not express major histocompatibility complex (MHC) class I molecules, CD8 T-cells cannot recognize CTAs expressed on them; this suggests that CTAs are the ideal tumor immunotherapy targets. In particular, NY-ESO-1 is the most immunogenic CTA discovered thus far, and is considered to be a highly promising therapeutic immunotherapy target [3]. It has been shown that the expression of NY-ESO-1 is reactivated in cancerous cells. This could be due to a loss of epigenetic regulation as observed when methylated chromatin regions are demethylated or deacetylated histones are acetylated [4]. Recently, we demonstrated that, while expression of NY-ESO-1 is not observed in human

glioma, the prototype inhibitor of DNA methylation, i.e., 5-aza-2′-deoxycytidine (DAC), markedly reactivates NY-ESO-1 expression in glioma cells, but not in normal human cells. In addition, glioma cells forcibly expressing NY-ESO-1 show in vitro and in vivo sensitivity to antigen-specific cytotoxic T lymphocytes (CTLs) [5].

It is widely accepted that histone modification and DNA methylation are intricately interrelated; these mechanisms act together to determine the status of gene expression. The synergistic effect of DNA demethylation and histone deacetylase (HDAC) inhibition has been investigated in greater detail [6–8]. DNA is wrapped around a core of eight histones to form nucleosomes, which constitute the smallest structural unit of chromatin. The basic amino-terminal tails of histones protrude out of the nucleosome and are subject to posttranslational modification, including histone acetylation and methylation. The acetylation status of lysine residues on histones H3 and H4 is controlled by the balanced action of the histone acetyltransferases (HATs) and histone deacetylase (HDAC). Acetylated histones have constantly been associated with transcriptionally active or open chromatin. In contrast, deacetylation status induced by HDACs results in chromatin compaction and gene inactivation. Histone methylation, mediated by histone methyltransferase (HMTs), exerts different effects on gene expression, depending on the target residue. In fact, while histone H3 lysine 9 (H3-K9) methylation marks transcriptionally inactive chromatin, methylation of H3-K4 is associated with transcriptionally active chromatin [9].

In order to maximally achieve gene reactivation, it may be necessary to simultaneously inhibit both DNA methylation and histone deacetylation. Inhibition of HDAC increases histone acetylation and induces the chromatin structure to adopt a more open conformation. This conformational change may lead to restoration of transcriptionally silenced pathways or suppression of aberrantly expressed genes via repressor protein recruitment [10]. Naturally occurring and synthetic HDAC inhibitors (HDACi) are a new generation of chemical agents being used to develop therapy against cancer and other diseases, including acquired immunodeficiency syndrome (AIDS) [11, 12]. Among a variety of HDACi discovered thus far, valproic acid (VPA), which was initially introduced as an anticonvulsant a few decades ago and was more recently introduced for the treatment of bipolar disorder, has been shown to inhibit HDAC at therapeutic plasma concentrations [13].

In this study, we investigated the synergistic effect of VPA and DAC on CTA reactivation in human glioma cells and examined the status of DNA methylation and histone modification in them.

Materials and methods

Cells

The human glioma cell lines U251 and T98 were derived originally at Memorial Sloan-Kettering Cancer Institute (New York, NY) and maintained in Eagle's minimal essential medium (MEM) at 37°C in an humidified atmosphere of 5% CO_2 in air. The human osteosarcoma cell line, SaOS-2 (NY-ESO-1$^+$), was kindly provided by Dr. Y. Nishida (Department of Orthopedics, Nagoya University, Nagoya, Japan) and maintained in Dulbecco's modified Eagle's medium (DMEM; Nissui, Tokyo, Japan). The medium was supplemented with 10% fetal bovine serum (FBS), 5 mM L-glutamine, 2 mM nonessential amino acids, and antibiotics (100 U/ml penicillin and 100 μg/ml streptomycin). Commercially available normal human astrocytes (NHA; Cambrex, Baltimore, MD) maintained in AGM medium with the BulletKit supplement (Cambrex) were used as normal brain cells.

In vitro treatment of cultured cells with DAC and VPA

Treatment with DAC was performed as described in our previous study [5]. Briefly, cells were seeded at a density of 1.0×10^5 cells/well in a six-well plate, and placed at 37°C overnight in a 5% CO_2 incubator. The next day, the cell culture medium was replaced with fresh medium containing 1 μM DAC (Sigma-Aldrich, St. Louis, MO). The medium was changed every 12 h for 2 days (four pulses). VPA was purchased from Sigma-Aldrich and dissolved in MEM. Treatment with VPA was performed at a final concentration of 0.5 mM every 24 h for 2 days (two pulses). Cells were treated with DAC alone, VPA alone, or a combination of both DAC and VPA. At the end of the treatment period the medium was replaced with fresh medium without agents and the cells were cultured for an additional 48 h before extracting RNA or DNA for analysis.

Conventional reverse-transcription PCR

Total RNA was prepared from cultured cells using the RNeasy Mini Kit (Qiagen, Hilden, Germany). cDNAs were synthesized from 1 μg total RNA using the Transcriptor First Strand cDNA Synthesis kit (Roche, Mannheim, Germany) according to the manufacturer's protocol. cDNA was then subject to polymerase chain reaction (PCR) using Go Taq DNA Polymerase (Promega, Madison, WI) as described previously [5]. The PCR primers used are listed in Table 1. Glyceraldehyde-3-phosphate dehydrogenase (GAPDH)-specific PCR products from the same RNA samples were amplified and served as internal controls. If no signal of NY-

ESO-1 was observed after a 35-cycle amplification, the remaining PCR products were amplified by an additional 15 cycles in order to confirm the absence of the signal.

Quantitative RT-PCR

After synthesis of the first cDNA strand as described above, quantitative RT-PCR was performed on LightCycler real-time RT-PCR system (version 3.39) (Roche), using the FastStart TaqMan Probe Master (ROX) (Roche) along with the sets of primers and Universal ProbeLibrary probes (Roche) listed in Table 1. Each sample was amplified as follows: 1 cycle at 95°C for 10 min followed by 45 cycles at 95°C for 15 s and 60°C for 1 min. cDNA from SaOS-2 was used to generate the standard curves for *NY-ESO-1* and *GAPDH*. Standardization of samples was achieved by dividing the copy number of the target gene by that of the *GAPDH* gene. Values were expressed as ratios relative to *NY-ESO-1* expression in SaOS-2.

Western blot analysis

Western blotting was performed using a monoclonal antibody (mAb) against NY-ESO-1 (ES121; Zymed, San Francisco, CA) as previously described [5]. Band intensities were quantified by densitometric scanning using the National Institutes of Health (NIH) IMAGE program.

NY-ESO-1 promoter DNA methylation analysis

Methylation-specific PCR (MSP) and Pyrosequencing™ technology were used to determine the methylation status of the CpG island region of *NY-ESO-1* as described previously [5]. The primer sequences are listed in Table 1. The primer sequences for Pyrosequencing™ were designed using PSQ Assay Design (Biotage, Uppsala, Sweden). A 50-μl PCR was carried out in 60 mM Tris ± HCl (pH 8.5), 15 mM ammonium sulfate, 2 mM $MgCl_2$, 10% DMSO, 1 mM dNTP mix, 1 U Taq polymerase, 5 pmol forward primer, 50 pmol reverse primer, 50 pmol biotinylated universal primer, and ~50 ng bisulfite-treated genomic DNA. The forward primer contains a 20-bp linker sequence on the 5′ end that is recognized by biotin-labeled primers; thus, the final PCR product can be purified using Sepharose beads. PCR cycling conditions were as follows: 95°C for 30 s, 60°C for 45 s, and 72°C for 45 s for 55 cycles. The biotinylated PCR product was purified as recommended by the manufacturer. In brief, the

Table 1 Primer sequences

		Sequence	TaqMan probe#
Conventional RT-PCR			
NY-ESO-1	Forward	CATCACGGATCCATGCAGGCCGAAGGCCGG	
	Reverse	ACCCGGGGTACCGCGCCTCTGCCCTGAGGG	
GAPDH	Forward	GACCACAGTCCATGCCATCAC	
	Reverse	GTCCACCACCCTGTTGCTGTA	
q-RT-PCR			
NY-ESO-1	Forward	TGTCCGGCAACATACTGACT	Human#67
	Reverse	ACTGCGTGATCCACATCAAC′	
GAPDH	Forward	AGCCACATCGCTCAGACAC	Human#60
	Reverse	CGCCCAATACGACCAAATC	
MSP			
Unmethylated NY-ESO-1	Forward	GTGTAGGGGTAGTAAGGGTTTT	
	Reverse	CAACTCAAACAAACAACTCTCCA	
Methylated NY-ESO-1	Forward	CGTAGGGGTAGTAAGGGTTTC	
	Reverse	ACTCAAACAAACGACTCTCCG	
Pyrosequencing	Forward	GGGTTGAATGGATGTTGTAG	
	Reverse	CRCCACCAAAACTATCAA	
	Biotinylated universal primer	GGGACACCGCTGATCGTTTACRCCAC CAAAACTATCAA	
	Pyrosequencing primer	TGAATGGATGTTGTAGATG	
CHIP-PCR	Left	ACCCGCAACCCACCCCACAC	
	Right	GGGGCAGGCCTCTAACTGGG	
CHIP-qPCR	Left	TTCCAGCTACCCCACCAG	Human#66
	Right	GGGGCAGGCCTCTAACTG	

PCR product was bound to Streptavidin Sepharose HP (Amersham Biosciences, Uppsala, Sweden), and the Sepharose beads containing the immobilized PCR product were purified, washed, denatured using 0.2 M NaOH solution, and washed again. Next, 0.3 mM pyrosequencing primer was annealed to the purified single-stranded PCR product, and pyrosequencing was performed using the PSQ HS 96Pyrosequencing System (Pyrosequencing, Inc., Westborough, MA). Methylation quantification was performed using the provided software.

CHIP assays

The protocols for chromatin immunoprecipitation (CHIP) have been described previously [14]. Briefly, cells were treated with 1% formaldehyde for 8 min to cross-link histones to DNA. After washing, the cell pellets were resuspended in 550 μl lysis buffer and sonicated seven times for 8 s each. The lysate (500 μl) was then divided into three fractions; the first and second ones (230 μl each) were diluted in 260 μl of lysis buffer, and the third one (40 μl) was used for input control. The first lysate was incubated with 10 μl anti-Lys-9 acetylated histone H3 antisera, or 10 μl anti-Lys-9 dimethylated H3 antibody (Upstate Biotechnology, Temecula, CA), or 10 μl anti-Lys-4-dimethylated H3 antibody (Upstate Biotechnology) at 4°C overnight. The second lysate was incubated with mock preimmune sera (10 μl) at 4°C overnight as the negative control. To collect the immunoprecipitated complexes, protein G-agarose beads (Active Motif, Carlsbad, CA) were added and incubated for 1.5 h at 4°C. After washing, the beads were treated with RNase and proteinase K. DNA was extracted using DNA purification minicolumns (Active Motif) and resuspended in 100 μl water. PCR amplification of DNA was carried out on diluted DNA aliquots, using the primers shown in Table 1. Quantification of CHIP DNA was performed in triplicate by real-time PCR by the LightCycler real-time RT-PCR system (version 3.39) (Roche), using the FastStart TaqMan Probe Master (ROX) (Roche) along with the sets of primers and Universal ProbeLibrary probes (Roche) listed in Table 1. Data were analyzed by Comparative C_T methods.

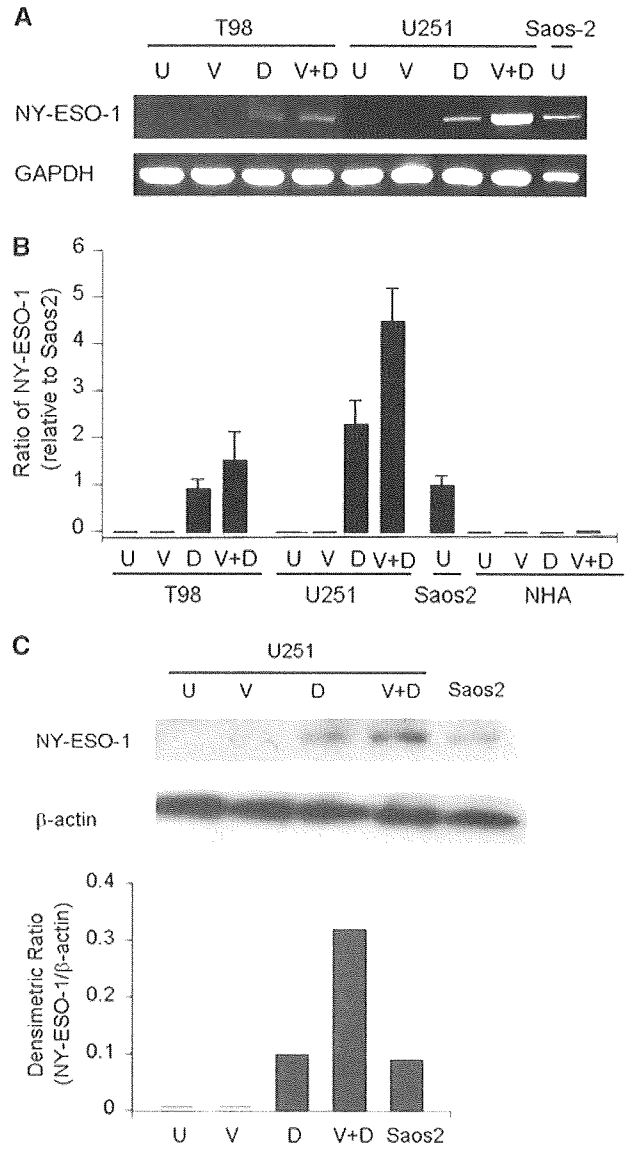

Fig. 1 Enhancement of *NY-ESO-1* expression by combination of VPA and DAC in glioma cells. **a** Conventional reverse-transcriptase polymerase chain reaction (RT-PCR). Osteosarcoma cell line, namely, SaOS-2, which expresses *NY-ESO-1* constitutively, was used as the positive control. **b** Real-time PCR. Ratio of *NY-ESO-1* amounts relative to SaOS-2 is expressed (the mean and SD of three experiments). Note that *NY-ESO-1* expression was not induced by any treatment in normal human astrocytes (NHA). **c** Western blot analysis. The histogram shows the amount of NY-ESO-1 relative to that of *β*-actin

Results

Enhancement of NY-ESO-1 expression in glioma cells by a combination of VPA and DAC (Fig. 1)

NY-ESO-1 expression was not detected in glioma cells treated with control agents or VPA alone. Consistent with the results of our previous study [5], we observed that DAC-alone treatment reproducibly elicited induction of the *NY-ESO-1* gene in the T98 and U251 cell lines. We investigated whether treatment with VPA, acting as an HDACi, enhanced the ability of DAC to reactivate *NY-ESO-1* gene expression. As shown in Fig. 1a, VPA treatment augmented DAC-mediated induction of NY-ESO-1 expression in the two cell lines. Although some variability regarding the magnitude of gene induction was noted in these two cell lines, the combination treatment

enhanced *NY-ESO-1* expression more than exposure to DAC alone. By contrast, DAC alone and even the combination of DAC and VPA did not induce *NY-ESO-1* expression in normal astrocyte line, namely, NHA. *NY-ESO-1*-specific bands were not observed even after 50-cycle PCR amplification. Real-time PCR revealed that the combination treatment of VPA and DAC resulted in an approximately 2- and 1.5-fold increase in *NY-ESO-1* expression relative to DAC alone in U251 and T98 cells, respectively (Fig. 1b). To assess whether the induction of *NY-ESO-1* mRNA is followed by the production of the appropriate protein, Western blotting for *NY-ESO-1* was performed in glioma cells. As shown in Fig. 1c, bands corresponding to *NY-ESO-1* were observed in U251 cells treated with DAC; however, these bands were absent in the cells treated with control agents or VPA alone. A denser band was observed in the cells treated with the combination of VPA and DAC. These results were consistent with those obtained with T98 cells. Taken together, these results indicate that *NY-ESO-1* expression is enhanced by combination of VPA and DAC in glioma cells.

Methylation status of the *NY-ESO-1* gene

MSP experiments were performed to evaluate the methylation status of *NY-ESO-1* in glioma cells. We observed that *NY-ESO-1* is heavily methylated in U251 cells treated with control agents or VPA alone. In contrast, bands corresponding to unmethylated alleles were observed in cells cultured with DAC and with combination of VPA and DAC (Fig. 2a). To quantify the methylation of the CpG sites of *NY-ESO-1*, we employed a novel real-time DNA sequencing technology called Pyrosequencing^{TM}. We identified the regions showing the largest differences in methylation and compared methylation levels within a small window (three CpG sites) of *NY-ESO-1*. Mean methylation levels ± standard deviation (SD) values were 89 ± 3% and 77 ± 9% for U251 treated with control agents and VPA, respectively. The difference was not statistically significant. However, DAC reduced the methylation level to 56 ± 5% ($P < 0.05$ compared with untreated cells). Interestingly, following treatment with the combination of VPA and DAC, the methylation level was further significantly decreased to 35 ± 6% ($P < 0.05$ compared with DAC alone) (Fig. 2b). VPA also had a small effect on *NY-ESO-1* promoter demethylation, perhaps through a replication-independent demethylation property of VPA acting with DAC. The MSP and Pyrosequencing data of other glioma cell lines were almost identical (data not shown).

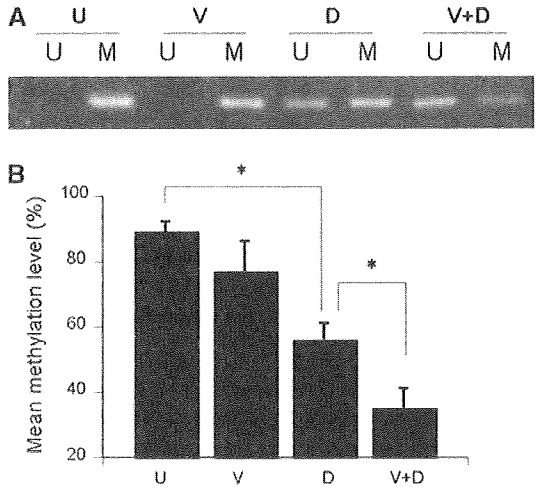

Fig. 2 Methylation status of the *NY-ESO-1* gene. **a** Methylation-specific polymerase chain reaction (PCR). *NY-ESO-1* is heavily methylated in U251 cells treated with control agents or valproic acid (VPA) alone. By contrast, bands corresponding to unmethylated alleles were observed in cells cultured in 5-aza-2′-deoxycytidine (DAC) and in a combination of VPA and DAC. **b** Quantitative pyrosequencing. DAC significantly reduced the methylation level. Interestingly, following treatment with the combination of VPA and DAC, the methylation level was further significantly decreased (*$P < 0.05$)

Histone modification

We determined whether the increase in expression in response to the combination of DAC and VPA is associated with gross changes in chromatin structure in the *NY-ESO-1* promoter region by chromatin immunoprecipitation (CHIP) assay and quantitative real-time chromatin-immunoprecipitation polymerase chain reaction (CHIP-PCR) in U251 glioma cells. In these assays, DNA combined with acetylated or methylated histone H3 Lys-9 (K9) antibody, or methylated H3 Lys-4 antibody is immunoprecipitated and detected by PCR amplification (Fig. 3a). Quantification of CHIP DNA was performed in triplicate by real-time PCR (Fig. 3b). The level of acetylated histone H3-K9 was increased by VPA and combination treatment as compared with untreated cells. DAC alone and the combination of DAC and VPA decreased the level of H3-K9 methylation. However, neither DAC nor VPA alone nor in combination affected K4-methylation. These results are considerably consistent with the findings that DAC reactivated *NY-ESO-1* in synergy with VPA, indicating that the induction of *NY-ESO-1* after DAC and VPA treatment is accompanied by a prominent increase in active histone marks around the transcription start sites of *NY-ESO-1* (Fig. 3c).

Discussion

Among the different tumor-associated antigens (TAA) identified, CTAs have attracted growing interest as

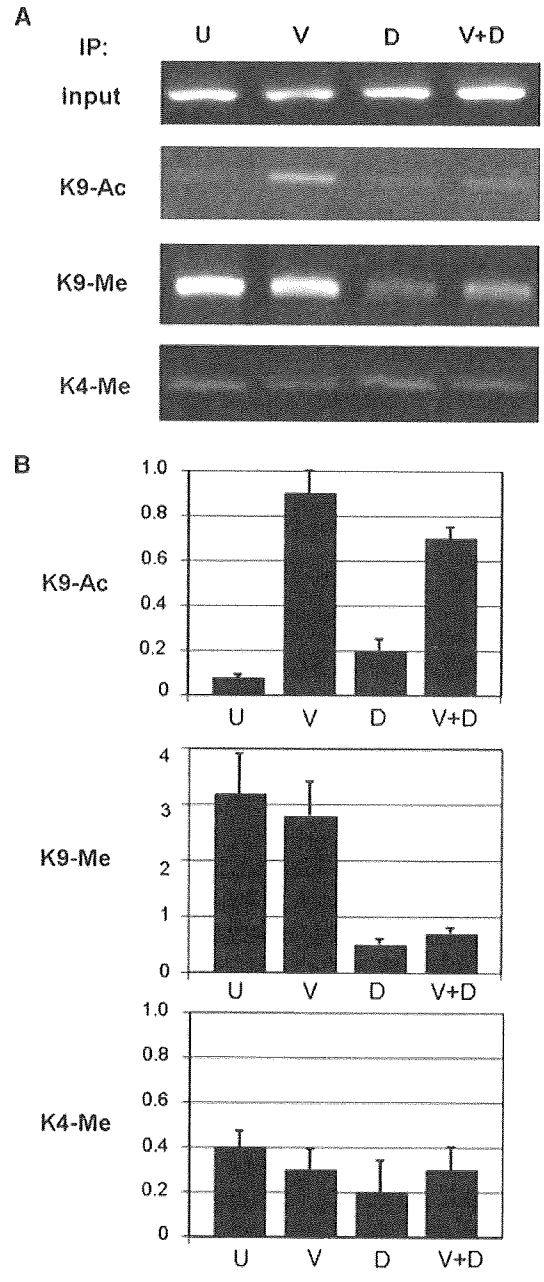

Fig. 3 Chromatin immunoprecipitation (CHIP) analysis of histone H3-lysine 9 acetylation (K9-Ac), lysine 9-dimethylation (K9-Me), and lysine 4-dimethylation (K4-Me). K9-Ac is considered to be associated with transcriptionally active or open chromatin. While K9-Me marks transcriptionally inactive chromatin, K4-Me is associated with transcriptionally active chromatin. **a** Conventional CHIP-polymerase chain reaction (PCR). **b** Quantitative real-time PCR using the TaqMan probe. Data represents ratio to input. Note that valproic acid (VPA) (V) and a combination of VPA and 5-aza-2′-deoxycytidine (DAC) (V + D) induced remarkable K9-Ac, and DAC (D) and a combination of VPA and DAC (V + D) remarkably decreased K9-Me while K4-Me was not affected by any treatment. **c** A schematic representation of the proposed mechanism in the role of histone modifications in the *NY-ESO-1* promoter. (i) Methylation in Lys-9, moderate methylation in Lys-4, and hypermethylation of the CpG islands cause a repressive folded chromatin structure, leading to *NY-ESO-1* gene silencing. (ii) VPA increases Lys-9 acetylation, but has no effect on Lys-9 methylation or Lys-4 methylation and does not relieve transcriptional silencing. (iii) DAC decreases Lys-9 methylation dramatically, demethylates the CpG sites, and opens chromatin structure, leading to reactivation of gene expression. (iv) The combination of DAC and VPA decreases Lys-9 methylation and increases Lys-9 acetylation. Lys-4 methylation is not affected. The combination opens chromatin to a considerable extent and reactivates gene expression with the greatest efficiency

immunotherapeutic targets due to their in vivo immunogenicity, their shared expression among tumors of different histotype, and their absence in normal tissues, except in the testis and the placenta. These characteristics bring them extremely close to being defined as tumor-restricted/specific antigens [3]. NY-ESO-1, one of the CTAs, was identified during a serological analysis of recombinant tumor cDNA expression libraries SEREX analysis of an esophageal cancer [1]. The gene for NY-ESO-1 maps to Xq28 and codes for an 18-kDa protein [15]. NY-ESO-1 appears to be one of the most immunogenic human tumor antigens defined to date. NY-ESO-1 mRNA expression is found in 20–30% of melanomas; lung, breast, ovarian, and bladder cancers; and other tumor types. However, we previously demonstrated that NY-ESO-1 is not observed in glioma [5]. Subsequent to our previous report showing DAC-mediated de novo induction of *NY-ESO-1* expression, we observed synergistic induction by the combination of DAC and VPA. This is the first report of such induction in glioma. We demonstrated that the combination resulted in decreasing levels of H3K9-diMe and increasing of H3K9-Ac levels accompanied with DNA demethylation on the *NY-ESO-1* promoter region. These data are consistent with the results of many previous intensive studies. We also examined the active mark (H3K4-diMe) on the same region. However, we did not find significant changes in this modification, suggesting that DNA methylation and H3-K9 modification are more dominantly associated with the expression of NY-ESO-1 than H3K4-diMe. A reason for the absence of close correlation between NY-ESO-1 expression and H3-K4 modification might be because of the fact that H3K4-diMe is associated with "permissive" chromatin that is either active or potentially active [16]. Nevertheless, our data is quite consistent with the findings that DAC reactivated *NY-ESO-1* in synergy with VPA. Thus, our results not only shed light on a potential epigenetic immunotherapy but also suggest that the silencing mechanism of *NY-ESO-1* in gliomas is mediated by both DNA methylation and histone modification.

Recent studies have shown that HDACs play an important role in the regulation of gene transcription and oncogenesis through remodeling of chromatin structure and dynamic changes in nucleosomal packing of DNA [10, 17, 18]. Inhibition of HDAC increases histone acetylation and maintains chromatin structure in a more open

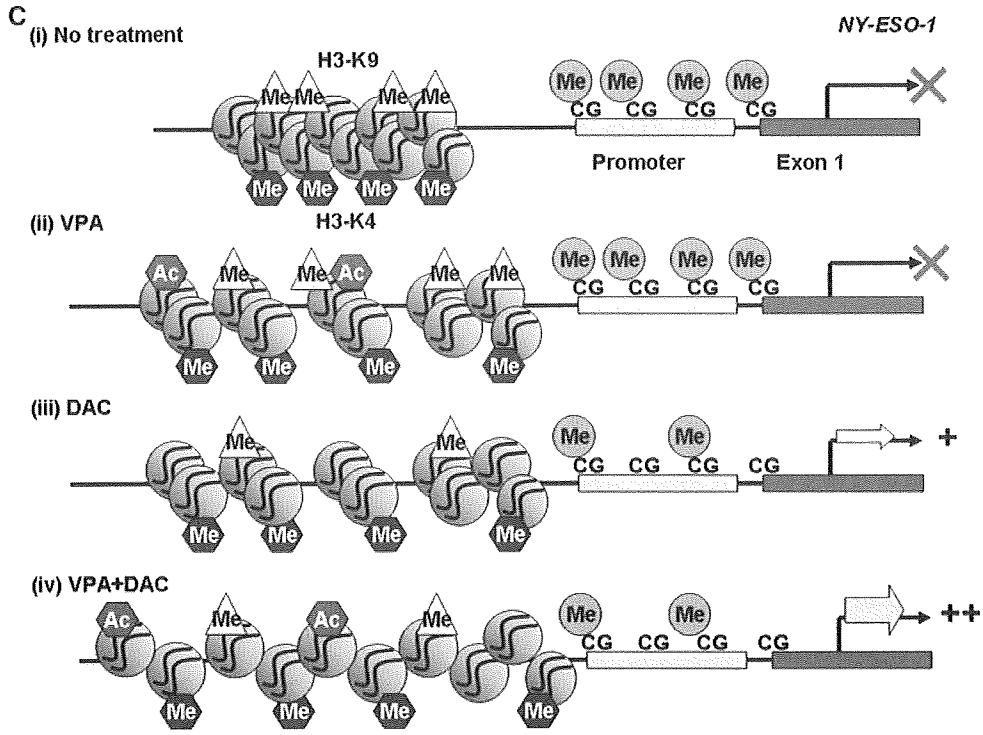

Fig. 3 continued

conformation. This conformational change may lead to restoration of transcriptionally silenced pathways or suppression of aberrantly expressed genes via repressor protein recruitment [10]. HDACi directly interacts with the catalytic site of HDAC, thereby blocking substrate access to the active Zn+ or NAD+ at its base [19, 20]. Inhibitors of zinc-dependent HDAC (class I, class II) have been the focus of intense research. Of these, the well-tolerated antiepileptic drug VPA, first synthesized in the 19th century, was observed to be a class I selective HDACi in 2001 [13, 18]. As expected for HDAC inhibitory compounds, VPA induces carcinoma cell differentiation. Since VPA has been used clinically for more than two decades, the pharmacology and side-effects of this drug have been studied in detail. VPA can pass across the BBB and has a long half-life of 9–20 h in humans. The therapeutic concentration of VPA in cerebrospinal fluid and plasma is in the range of 0.5–1 mM, in concordance with the level used in our experiments. This concentration is also considered therapeutic in the routine treatment of bipolar disorder.

In conclusion, we have investigated the efficacy of combinations of low concentrations of VPA with DAC on the expression of NY-ESO-1 antigen and the HDAC inhibitory activity of VPA via promoter demethylation and histone acetylation in glioma cells. The combined treatment of DAC and VPA as an effective HDACi was shown to increase *NY-ESO-1* expression in synergy; this suggests that this combination may be a novel strategy for immunotherapy in glioma patients. This combination therapy is currently being considered for further investigation in clinical trials.

References

1. Chen YT, Scanlan MJ, Sahin U et al (1997) A testicular antigen aberrantly expressed in human cancers detected by autologous antibody screening. Proc Natl Acad Sci USA 94:1914–1918. doi:10.1073/pnas.94.5.1914
2. Boon T, Cerottini JC, Van den Eynde B et al (1994) Tumor antigens recognized by T lymphocytes. Annu Rev Immunol 12:337–365. doi:10.1146/annurev.iy.12.040194.002005
3. Jager E, Nagata Y, Gnjatic S et al (2000) Monitoring CD8 T cell responses to NY-ESO-1: correlation of humoral and cellular immune responses. Proc Natl Acad Sci USA 97:4760–4765. doi:10.1073/pnas.97.9.4760
4. dos Santos NR, Torensma R, de Vries TJ et al (2000) Heterogeneous expression of the SSX cancer/testis antigens in human melanoma lesions and cell lines. Cancer Res 60:1654–1662
5. Natsume A, Wakabayashi T, Tsujimura K et al (2008) The DNA demethylating agent 5-aza-2′-deoxycytidine activates NY-ESO-1 antigenicity in orthotopic human glioma. Int J Cancer 122:2542–2553
6. Cameron EE, Bachman KE, Myohanen S et al (1999) Synergy of demethylation and histone deacetylase inhibition in the re-expression of genes silenced in cancer. Nat Genet 21:103–107. doi:10.1038/5047
7. Nguyen CT, Weisenberger DJ, Velicescu M et al (2002) Histone H3-lysine 9 methylation is associated with aberrant gene silencing in cancer cells and is rapidly reversed by 5-aza-2′-deoxycytidine. Cancer Res 62:6456–6461

8. Suzuki H, Gabrielson E, Chen W et al (2002) A genomic screen for genes upregulated by demethylation and histone deacetylase inhibition in human colorectal cancer. Nat Genet 31:141–149. doi:10.1038/ng892
9. Cheung P, Lau P (2005) Epigenetic regulation by histone methylation and histone variants. Mol Endocrinol 19:563–573
10. Richon VM, O'Brien JP (2002) Histone deacetylase inhibitors: a new class of potential therapeutic agents for cancer treatment. Clin Cancer Res 8:662–664
11. Egger G, Liang G, Aparicio A et al (2004) Epigenetics in human disease and prospects for epigenetic therapy. Nature 429:457–463. doi:10.1038/nature02625
12. Lehrman G, Hogue IB, Palmer S et al (2005) Depletion of latent HIV-1 infection in vivo: a proof-of-concept study. Lancet 366:549–555. doi:10.1016/S0140-6736(05)67098-5
13. Phiel CJ, Zhang F, Huang EY et al (2001) Histone deacetylase is a direct target of valproic acid, a potent anticonvulsant, mood stabilizer, and teratogen. J Biol Chem 276:36734–36741. doi:10.1074/jbc.M101287200
14. Kondo Y, Shen L, Issa JP (2003) Critical role of histone methylation in tumor suppressor gene silencing in colorectal cancer. Mol Cell Biol 23:206–215. doi:10.1128/MCB.23.1.206-215.2003
15. Chen YT, Boyer AD, Viars CS et al (1997) Genomic cloning and localization of CTAG, a gene encoding an autoimmunogenic cancer-testis antigen NY-ESO-1, to human chromosome Xq28. Cytogenet Cell Genet 79:237–240. doi:10.1159/000134734
16. Santos-Rosa H, Schneider R, Bannister AJ et al (2002) Active genes are tri-methylated at K4 of histone H3. Nature 419:407–411. doi:10.1038/nature01080
17. Marks PA, Miller T, Richon VM (2003) Histone deacetylases. Curr Opin Pharmacol 3:344–351. doi:10.1016/S1471-4892(03)00084-5
18. Gottlicher M, Minucci S, Zhu P et al (2001) Valproic acid defines a novel class of HDAC inhibitors inducing differentiation of transformed cells. EMBO J 20:6969–6978. doi:10.1093/emboj/20.24.6969
19. Marks P, Rifkind RA, Richon VM et al (2001) Histone deacetylases and cancer: causes and therapies. Nat Rev 1:194–202
20. Acharya MR, Sparreboom A, Venitz J et al (2005) Rational development of histone deacetylase inhibitors as anticancer agents: a review. Mol Pharmacol 68:917–932. doi:10.1124/mol.105.014167

Clin J Gastroenterol (2009) 2:222–225
DOI 10.1007/s12328-009-0071-2

CASE REPORT

Total pancreatectomy for multiple neuroendocrine tumors of the pancreas in a patient with von Hippel–Lindau disease

Hiromichi Maeda · Isao Nishimori · Takehiro Okabayashi · Takuhiro Kohsaki · Taro Shuin · Michiya Kobayashi · Saburo Onishi · Kazuhiro Hanazaki

Received: 7 January 2009 / Accepted: 16 February 2009 / Published online: 19 March 2009

Abstract Von Hippel–Lindau disease (VHLD) is an autosomal dominant familial syndrome associated with multiple neoplasms. Medical management of pancreatic lesions is still controversial, especially for pancreatic neuroendocrine tumors (NET). We report an experience of total pancreatectomy for multiple pancreatic neuroendocrine tumors in a VHLD patient, and discuss the indication of surgical treatment. The patient was a 33-year-old Japanese female with a medical history of VHLD-associated tumors. At 27 years of age, abdominal computed tomography revealed a number of strongly enhanced round tumors throughout the pancreas. She underwent total pancreatectomy with portal vein resection because of back pain and an increase of tumor size. Pathological examination reconfirmed the diagnosis of multiple pancreatic NET invading the portal vein. She has been well with intensive insulin therapy and has shown no recurrence of NET for more than one year. This is a rare case of total pancreatectomy with portal vein resection for treatment of pancreatic NET in a VHLD patient. Total pancreatectomy is a viable option for treatment of multi-centric or extensive pancreatic NET because of a favorable prognosis of NET after radical surgical treatment.

H. Maeda • T. Okabayashi • M. Kobayashi • K. Hanazaki
Department of Surgery, Kochi Medical School,
Okocho, Nankoku, Kochi, Japan

I. Nishimori (&) • T. Kohsaki • S. Onishi
Department of Gastroenterology and Hepatology,
Kochi Medical School, Okocho,
Nankoku, Kochi 783-8505, Japan
e-mail: nisao@kochi-u.ac.jp

T. Shuin
Depatment of Urology, Kochi Medical School,
Okocho, Nankoku, Kochi, Japan

Keywords Von Hippel–Lindau disease (VHLD) • VHL gene • Mutation • Neuroendocrine tumor • Total pancreatectomy

Introduction

Von Hippel–Lindau disease (VHLD) is an autosomal dominant familial disorder caused by a germline mutation of the VHL tumor suppressor gene, and is characterized by benign and malignant tumors affecting multiple organs, including the central nervous system, kidney, adrenal grand, pancreas, and reproductive system [1]. The pancreatic lesions occur in 40–60% of VHLD patients and they are mostly cystic with a notable incidence of serous cystadenoma [1–3], a benign tumor without need for specific treatment [1].

By contrast, pancreatic neuroendocrine tumors (NET) occur in 8–18% of VHLD patients [1, 2]. In VHLD disease patients, NET are exclusively hormone-inactive [1–3], and surgical treatment is sometimes required to prevent local invasion and distant metastasis. However, when surgery should be recommended and what type of surgery should be chosen are still problems.

Case study

A 33-year-old Japanese woman had suffered back pain for seven years. She was referred to our institute because multiple solid tumors in the pancreas had gradually increased in size, which was pointed out at 27 years of age. She had a medical history of treatment for a variety of VHLD-associated tumors, including a pancreatic NET surgically resected at 14 years of age, hemangiomas of the

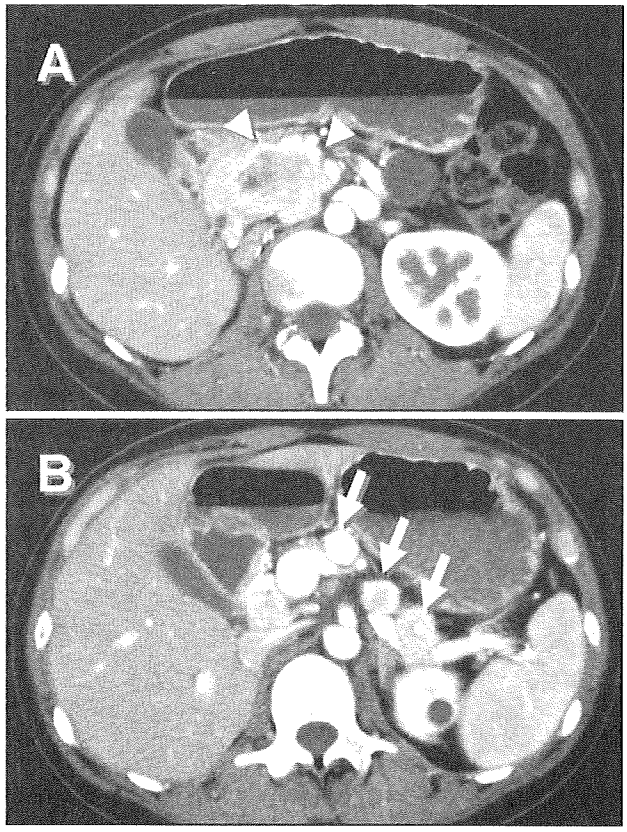

Fig. 1 Contrast-enhanced abdominal computed tomography. a The mass in the pancreatic head is heterogeneously enhanced and appears to invade the portal vein (arrowheads). b Multiple pancreatic masses are shown in the pancreatic body and tail (arrows) and are heterogeneously enhanced

fourth ventricle and cervical spinal cord operated at 19 years of age, and a renal cell carcinoma of the right kidney treated by nephrectomy at 30 years of age.

Mutational analysis of the VHL gene, performed using DNA extracted from her peripheral blood cells according to a previously reported method [4], revealed a G-to-A point mutation at nucleotide 500 (exon 1) resulting in an Arg167Glu amino acid substitution. Her father and elder brother were also diagnosed with VHLD, with her father having a medical history of two surgical resections for pancreatic NET and associated metastatic recurrence in the liver.

Blood tests showed increased serum levels of amylase (146 U/l, normal range; 40–115 U/l) and lipase (121 U/l, normal range; 13–60 U/l). There was no abnormality in serum levels for gastrointestinal and pancreatic hormones and tumor markers for NET, such as neuron-specific enolase. Abdominal computed tomography (CT) revealed multiple solid mass lesions throughout the pancreas (Fig. 1). These lesions were round with irregular alignment, strongly enhanced at the marginal region, and heterogeneously enhanced within the tumors. The tumor in the pancreatic head had a maximum diameter of 4.1 cm and appeared to invade the portal vein (Fig. 1a). Positron emission tomography with [^{18}F]fluorodeoxyglucose (FDG-PET) and FDG-PET-CT revealed positive signals for FDG accumulation in the pancreas, but no significant signal in other organs (Fig. 2). The maximum standardized uptake value (SUVmax) is high and differs among tumors, ranging from 9.0 to 16.3. Endoscopic retrograde cholangiopancreatogram failed to show the main pancreatic duct, but demonstrated narrowing of the common bile duct because of compression by the tumor in the pancreatic head. Fine needle aspiration biopsy was not performed because of the risk of hemorrhage from the tumor with abundant blood flow shown by the abdominal CT.

She underwent total pancreatectomy and the preoperative diagnosis was multiple malignant NET. Laparotomy revealed that the mass of the pancreatic head had partly invaded the portal vein but was totally removed by portal vein resection. Pathological investigation of the resected specimen showed that the mass lesion was composed of round tumor cells with oval nuclei and slightly eosinophilic cytoplasm growing in a nested pattern and surrounded by an abundance of blood vessels (Fig. 3a). The tumor cells had invaded the wall of the portal vein, but had not eroded the inner surface (Fig. 3b). No metastasis in peripancreatic lymph nodes was found. Immunohistochemical studies revealed that the tumor cells were positive for synaptophysin and chromogranin A. Mitosis was rarely observed, but positive staining for Ki-67 was observed in 1–10% of tumor cells. Taken together, these findings provide evidence for diagnosis of well-differentiated neuroendocrine carcinoma according to the WHO classification system.

Following the operation, watery diarrhea appeared because of pancreatic exocrine insufficiency, but subsided with oral administration of a large amount of digestive enzymes. She was discharged on the 30th postoperative day. She has been well with intensive insulin therapy and has shown no recurrence of NET for one year.

Discussion

To our knowledge, this is the third reported case of a VHLD patient with pancreatic NET that was treated with total pancreatectomy. Total pancreatectomy is a rarely chosen treatment option for pancreatic NET in VHLD patients. A large study of 633 VHLD patients from a single institute reported only two total pancreatectomies among 39 patients who underwent definitive pancreatic surgery [2]. Total pancreatectomy combined with portal vein resection, as performed in our case, for pancreatic NET in a

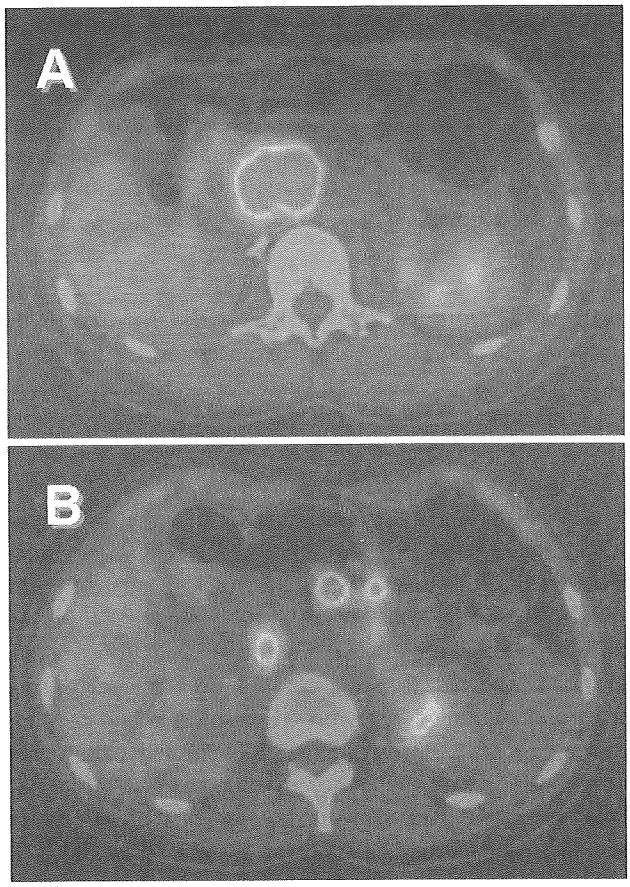

Fig. 2 [^{18}F]fluorodeoxyglucose-positron emission tomography with computed tomography. A number of positive signals for [^{18}F]fluorodeoxyglucose accumulation are seen in the entire pancreas. The SUVmax ranges from 9.0 to 16.3

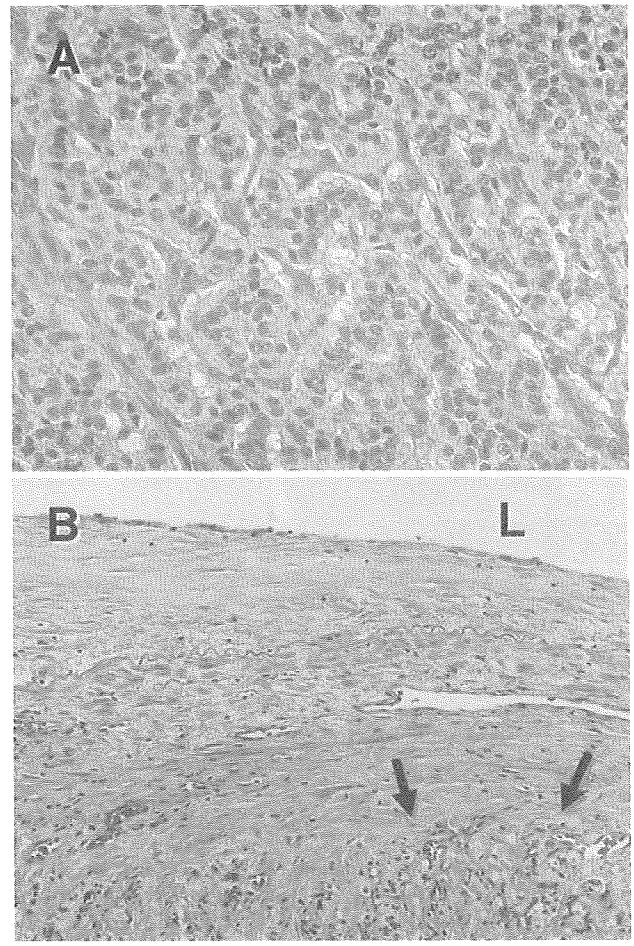

Fig. 3 Pathological examination. a The tumor is composed of round cells growing in a nested pattern and surrounded by an abundance of blood vessels. b Tumor cells invade the wall of the portal vein (arrows) but do not erode the inner surface of the portal vein. L, lumen of the portal vein

VHLD patient is extremely rare, and provides an invaluable instance of successful radical surgical treatment.

Generally, VHLD patients are subjected to many surgical operations during their lifetime, because of the occurrence and recurrence of a variety of tumors in various organs. Therefore surgical treatment may be avoided and careful observation may be chosen. However, operation is necessary when the tumor has high malignancy potential, because it improves the prognosis of patients with malignant pancreatic NET [5, 6].

In this case, the radiological images were suggestive of malignant nature of pancreatic NET. First, the size of the tumor was large with the maximum diameter of 4.1 cm. When the tumor size is greater than 3 cm, the tumor has an increased risk of liver metastasis and a shorter doubling time [2, 3]. Second, the pancreatic NETs were enhanced heterogeneously on CT. Typically, contrast-enhanced CT demonstrates pancreatic NET as a homogeneously hypervascular mass. In the present case, however, the tumor is heterogeneously enhanced, which possibly reflects the irregularity of the vascular structure, perfusion, and permeability, and also necrosis within the tumor, indicating the malignant potential of the pancreatic NET [3]. Third, the significant accumulation of FDG in pancreatic NET was demonstrated on FDG-PET-CT. A positive signal suggests that a tumor is likely malignant with high proliferative activity, while indolent pancreatic NET generally fails to show a positive signal [7].

A mutation in exon 3 of the VHL gene is reported to be associated with the malignant potential of pancreatic NET [2]. Our case showed a mis-sense mutation in exon 1, but not in exon 3 of the VHL gene. Further investigation of genotype–phenotype correlations with a large number of patients may provide the information necessary to determine the appropriate treatment option for pancreatic NET in VHLD patients.

In cases when surgical treatment is required, less-invasive surgery should be chosen to maximize preservation of pancreatic and neighboring organ function [8]. In the

present case, however, the pancreatic tumors in the body and tail displayed heterogeneous enhancement, which is similar to the tumor in the pancreatic head. For this reason, the decision was made to resect all tumors by total pancreatectomy.

In conclusion, total pancreatectomy with portal vein resection was successfully achieved in a VHLD patient with pancreatic NET. The postoperative course was uneventful and the patient has been well more than one year after the surgery. Radical and curative resection should be considered for treatment of malignant pancreatic NET to improve the prognosis of VHLD patients with pancreatic NET.

References

1. Lonser RR, Glenn GM, Walther M, Chew EY, Libutti SK, Linehan WM, et al. von Hippel–Lindau disease. Lancet. 2003;361:2059–67.
2. Blansfield JA, Choyke L, Morita SY, Choyke PL, Pingpank JF, Alexander HR, et al. Clinical, genetic and radiographic analysis of 108 patients with von Hippel–Lindau disease (VHL) manifested by pancreatic neuroendocrine neoplasms (PNETs). Surgery. 2007; 142:814–8.
3. Marcos HB, Libutti SK, Alexander HR, Lubensky IA, Bartlett DL, Walther MM, et al. Neuroendocrine tumors of the pancreas in von Hippel–Lindau disease: spectrum of appearances at CT and MR imaging with histopathologic comparison. Radiology. 2002;225:751–8.
4. Yoshida M, Ashida S, Kondo K, Kobayashi K, Kanno H, Shinohara N, et al. Germ-line mutation analysis in patients with von Hippel–Lindau disease in Japan: an extended study of 77 families. Jpn J Cancer Res. 2000;91:204–12.
5. Norton JA, Kivlen M, Li M, Schneider D, Chuter T, Jensen RT. Morbidity and mortality of aggressive resection in patients with advanced neuroendocrine tumors. Arch Surg. 2003;138:859–66.
6. Heidt DG, Burant C, Simeone DM. Total pancreatectomy: indications, operative technique, and postoperative sequelae. J Gastrointest Surg. 2007;11:209–16.
7. Bombardieri E, Maccauro M, De Deckere E, Savelli G, Chiti A. Nuclear medicine imaging of neuroendocrine tumours. Ann Oncol. 2001;12:S51–61.
8. Maeda H, Okabayashi T, Nishimori I, Kobayashi M, Sugimoto T, Kohsaki T, et al. Duodenum-preserving pancreatic head resection for pancreatic metastasis from renal cell carcinoma: a case report. Langenbecks Arch Surg. 2007;392:649–52.

〔VI〕

VHL病診断治療ガイドライン(案)

フォン・ヒッペルリンドウ(VHL)病の経過観察と診断治療指針(案)

平成２１年度 厚生労働科学研究費補助金

難治性疾患克服研究事業研究奨励分野

「ﾌｫﾝ･ﾋｯﾍﾟﾙﾘﾝﾄﾞｳ病の病態調査と診断治療系確立の研究」班

（２０１０年2月５日）

研究代表者

高知大学教育研究部医療学系泌尿器科学

執印太郎

厚生労働省科学研究費補助金難治性疾患克服研究事業
「フォン・ヒッペルリンドウ病の病態調査と診断治療系確立の研究」班

研究代表者

執印　太郎　　高知大学教育研究部医療学系泌尿器科学

研究分担者

澤村　豊　　北海道大学病院神経外科
西川　亮　　埼玉医科大学国際医療センター　脳神経外科
菅野　洋　　横浜市立大学医学部　脳神経外科
若林　俊彦　　名古屋大学大学院医学系研究科
脳神経病態制御学講座　脳神経外科
倉津　純一　　熊本大学大学院医学薬学研究部
先端生命医療科学部門　脳・神経科学講座
脳神経外科学分野
篠原　信雄　　北海道大学大学院医学研究科腎泌尿器外科学分野
矢尾　正祐　　横浜市立大学医学部泌尿器科学教室
米谷　新　　埼玉医科大学眼科
福島　敦樹　　高知大学教育研究部医療学系眼科学
西森　功　　高知大学医学部附属病院光学医療診療部
西森医院
伊藤　鉄英　　九州大学病院肝臓膵臓胆道内科

目次